Available online at www.sciencedirect.com
ScienceDirect
Earth and Planetary Science Letters 256 (2007) 1 – 11
EPSL
www.elsevier.com/locate/epsl

A view into the Cretaceous geomagnetic field from analysis of gabbros and submarine glasses

Roi Granot [a,*], Lisa Tauxe [a], Jeffrey S. Gee [a], Hagai Ron [b]

[a] *Scripps Institution of Oceanography, La Jolla, CA 92093, USA*
[b] *Institute of Earth Sciences, Hebrew University of Jerusalem, Jerusalem 91904, Israel*

Received 14 August 2006; received in revised form 23 December 2006; accepted 24 December 2006
Available online 5 January 2007
Editor: M.L. Delaney

Abstract

The nature of the geomagnetic field during the Cretaceous normal polarity superchron (CNS) has been a matter of debate for several decades. Numerical geodynamo simulations predict higher intensities, but comparable variability, during times of few reversals than times with frequent reversals. Published geomagnetic paleointensity data from the CNS are highly scattered suggesting that additional studies are required. Here we present new paleointensity results from 18 sites collected from the lower oceanic crust of the Troodos ophiolite, Cyprus (92.1 Ma old). Together with recently published data from the Troodos upper crust we obtain three independent paleointensity time-series. These sequences reveal quasi-cyclic variations of intensities about a mean value of 54±20 Z Am^2, providing insight into the fluctuating nature of the Cretaceous magnetic field. Our data suggest the CNS field was both weaker and more variable than predicted by geodynamo simulations. The large amplitudes of these variations may explain the wide range of dipole moments previously determined from the CNS.

Keywords: Cretaceous normal polarity superchron; paleointensity; Troodos ophiolite; paleomagnetism; geomagnetic field

1. Introduction

Convection within the liquid metal outer core is believed to generate the geomagnetic field [1]. Recent geodynamo numerical simulations have shown that heat flux distribution at the core–mantle boundary has a profound influence on the efficiency of convection within the core and therefore, on the character of the magnetic field [2,3]. In particular, the simulations predict that prolonged features in the history of the field, such as long times of stable polarity (superchrons), are controlled by the lower mantle thermal structure and ought to correspond with a high efficiency dynamo. They also predict that superchrons would be associated with an elevated dipole moment but comparable variability relative to times of high reversal frequency [2]. These predictions can be tested using geomagnetic paleointensity data from the Cretaceous normal polarity superchron (CNS, 120.6 to 83 Ma [4,5]).

Studies of the CNS using both volcanic and sedimentary rocks have lead to strikingly different conclusions regarding the strength and variability of the geomagnetic field (e.g., [6–15]). Some studies suggest rather low average moments (17 Z (10^{21}) Am^2 [6,7]) while others have moments as high as 190 Z Am^2

* Corresponding author.
E-mail address: rgranot@ucsd.edu (R. Granot).

0012-821X/$ - see front matter © 2007 Elsevier B.V. All rights reserved.
doi:10.1016/j.epsl.2006.12.028

[8–10]. This range of dipole moments is similar to that observed during the Cenozoic, a time with high reversal frequency [16]. Moreover, some studies have suggested low variability of the field (10% of the mean, [17]) while others displayed substantially higher variability (55% of the mean, [10]).

The controversy regarding the nature of the geomagnetic field during the CNS could result either from inadequate sampling of the field [13] or from unreliable data, or both. However, there is now a rather large body of published data, much of which conforms to the highest experimental standards. The current debate therefore revolves around selection criteria and the reliability of various recording media [18].

One heretofore unavailable tool to assess the reliability of absolute paleointensity data in the CNS is the degree to which sequential data points display serial correlation. Several sedimentary relative paleointensity records have been produced [14,15], but time-series of absolute paleointensity data from the CNS have not been available and in fact are difficult to obtain. If such a serial correlation could be demonstrated, the geomagnetic origin of the observed variation, as opposed to "noise" would be strongly supported. The magnetization of the oceanic crust as evidenced in magnetic anomaly amplitudes [19–21] may provide a means of obtaining geomagnetic intensity fluctuations but such data are presently insufficient for the CNS. Here we examine paleointensity variations in samples from the oceanic crust exposed in the Troodos ophiolite.

The Troodos ophiolite on the island of Cyprus offers a remarkable exposure of a portion of the oceanic crust dated with uranium–lead as being late Cretaceous in age (92.1 Ma, [22]). Extensive normal faulting and hydrothermal massive sulfide bodies exposed across most of the ophiolite are consistent with crustal formation at a slow to intermediate spreading center (full spreading rate of 20–75 mm/yr) [23–27]. The lower oceanic crust within this kind of spreading environment typically comprises discrete, short-lived, magma bodies (i.e., cooling units) [28].

The Troodos ophiolite comprises a complex tectonic framework with several ancient spreading axes penetrating into previously existing crust [29,30] (Fig. 1). The locations of the fossil spreading axes, representing the youngest rocks, are constrained by several independent structural observations. Blocks of sheeted dikes with opposite tilt and axial extensional faults mark the upper crustal exposure of the spreading axes [29,31]. The location of the spreading axis in the lower crust is more difficult to establish. Granot et al. [32] delineate the axis in the lower crust by using remanence data to identify lower crustal blocks that are decoupled from the upper crust. The chronological relations between the different structural domains are poorly constrained, but within a single domain lower crustal samples can be placed in a relative temporal framework using distance from the inferred spreading center as a proxy for the arrow of time. Moreover, there are several pseudo-stratigraphic sections through

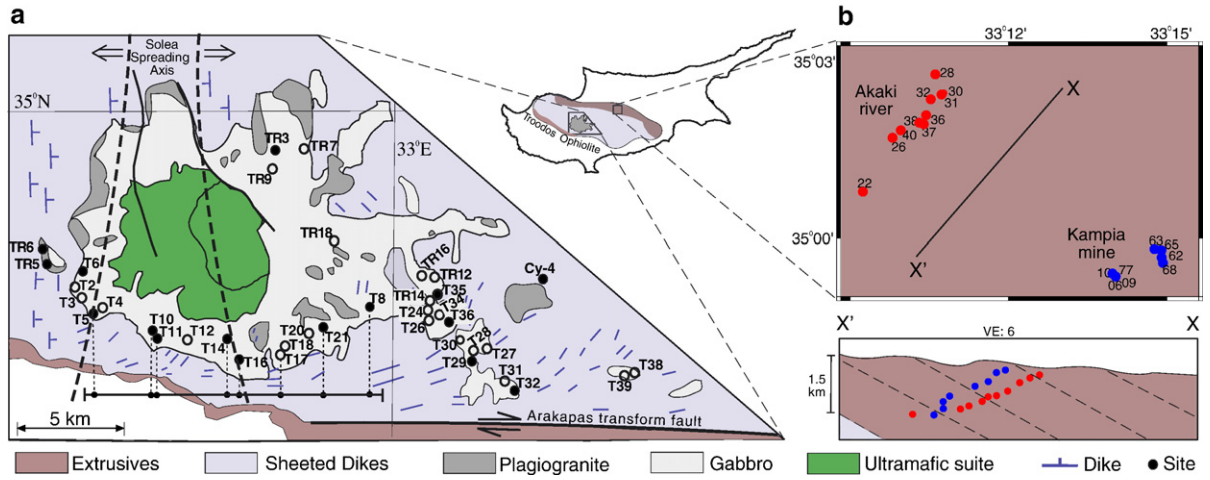

Fig. 1. Sampling sites from the Troodos ophiolite, Cyprus. (a) Gabbro sampling sites within the central intrusive suite. Heavy dashed lines and arrows indicate the location of the paleospreading axis and spreading direction, respectively. The axial location is inferred where minor lower crustal rotations occurred [32]. Solid (open) circles are the successful (unsuccessful) paleointensity sites. The fine dashed lines indicate the projections used to determine the distance of successful paleointensity sites along a flow line (shown in Fig. 3a). Distance along the flow-line is measured from the center of the Solea spreading axis. (b) Glass sampling sites (top) [10], and a schematic cross section through the extrusive sampled section (bottom). Their corresponding paleointensity time-series are shown in Fig. 3a.

the upper crust that also allow temporal ordering of cooling units.

For a time-series through the lower crust, we seek a coherent slice of gabbro in which relative age is well constrained. Deformation of the upper crust sheeted dikes [33,31] and rotations within the lower crust [32] imply that a coherent slice of crust is exposed near the intersection of the Solea spreading center and the Arakapas transform fault (Fig. 1). This slice contains the Solea spreading axis and extends some 6 km to the east (remanence data from lower crustal samples east of this slice (Granot, unpublished data) suggest that these eastern sites formed within a different spreading environment). Exposures of the gabbros parallel to the spreading direction within this coherent slice offer the possibility of constructing a temporal record of the Cretaceous geomagnetic field. Although the spatial variability of magma injection in the accretion zone [28] limits the temporal resolution, the distance of the gabbro sites from the spreading axis should provide an approximate temporal order. Here we consider only intensity variations in these gabbros; variations in remanence directions have been discussed by [32].

A second opportunity for temporal ordering is in the exposures of the upper crust in the Akaki Canyon and the Kampia mine area (Fig. 1). Tauxe and Staudigel [10] presented a large collection of data from these sections which we re-examine in terms of their spatio/temporal relationships.

In this study we present new data from 221 gabbroic samples obtained from 35 sites in the lower Troodos crust (Fig. 1), many of which can be located with respect to the ancient spreading center, and hence form a time-series. The Cyprus drilling project, CY-4, provides 12 additional sampling units of gabbroic material which contribute to the data set as a whole, but which cannot be

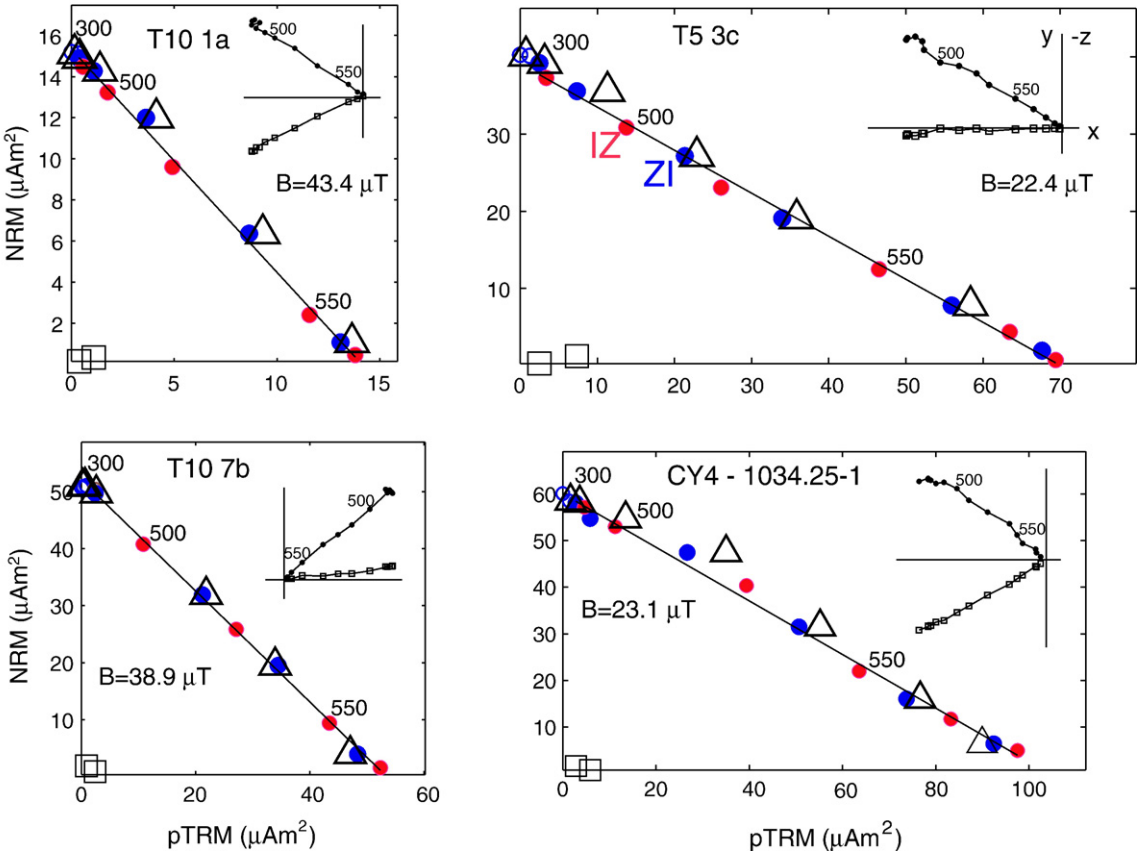

Fig. 2. Plots of representative examples of the modified Thellier–Thellier (IZZI) experiments on the Troodos lower crustal gabbros. Blue (red) symbols are the ZI (IZ) steps. Triangles and squares indicate pTRM checks and pTRM tail checks, respectively. Black line is the "best-fit" line over the temperature range used to estimate the intensity of the geomagnetic field. Insets show the corresponding vector end-point diagrams in specimen coordinates. Open and closed symbols indicate projections on the vertical and horizontal planes, respectively. (For interpretation of the references to colour in this figure legend, the reader is referred to the web version of this article.)

Table 1
Summary of paleointensity results

Specimen	T_1 (°C)	T_2 (°C)	N	$B_{anc.}$ (μT)	MAD	f_{vds} (%)	q	pTRM tail	DRATs	DANG (°)	β	VADM (Z Am^2)	R	VADM$_{AARM}$ (Z Am^2)
T5-3a	400	570	11	20.4	2.6	82	27.0	2.9	12	1.3	0.03	45.3		
T5-3b	300	570	12	19.1	2.9	89	26.3	1.3	12	1.1	0.03	42.4		
T5-3c	300	570	12	22.4	3.6	86	47.4	2.8	16	1.3	0.01	49.7		
T5-4a	400	570	11	17.9	2.7	80	25.6	6.2	18	1.2	0.03	39.7	I	
T5-4b	300	560	10	16.9	4.8	78	13.6	5.5	9	1.0	0.06	37.6		
T5-4cc	400	570	11	21.3	3.6	81	39.5	1.6	16	3.3	0.02	47.4	I	
T5-6b	300	570	12	26.0	2.5	89	35.7	1.8	10	1.6	0.02	57.9	I	
T5-7a	450	570	10	20.0	2.1	76	18.2	1.9	8	3.5	0.04	44.6		
T5-7bc	400	575	12	23.8	2.5	80	30.4	9.1	15	2.2	0.02	53.0	1.008	52.5
T5-7cc	400	570	11	25.4	3.4	83	32.0	1.6	15	2.4	0.02	56.5	I	
T6-11	450	575	11	58.3	2.0	87	36.6	1.3	18	0.5	0.02	130	I	
T6-12	450	575	11	60.6	1.8	86	65.9	0.9	22	0.8	0.01	135	I	
T6-13	450	575	11	56.6	1.1	86	28.8	1.0	15	1.2	0.02	126		
T6-14	450	575	11	61.6	2.0	89	63.5	1.9	10	0.2	0.01	137		
T6-51	520	575	9	43.2	2.8	78	17.6	1.6	22	2.7	0.04	96.2	I	
T6-54	450	575	11	52.7	2.7	83	32.5	4.4	13	0.8	0.02	117		
T8-31	400	555	8	26.3	3.4	75	18.3	6.1	22	3.5	0.03	58.5		
T8-33	500	565	8	27.3	4.1	67	9.25	4.4	21	4.0	0.06	60.7		
T8-34	300	560	10	29.7	3.6	80	16.9	4.7	13	3.7	0.04	66.1	I	
T8-35	450	570	10	19.2	4.9	76	12.9	4.0	16	4.3	0.06	42.6		
T8-51	300	560	10	26.0	3.4	82	15.4	3.3	23	3.2	0.05	57.8		
T10-1a	300	560	10	43.4	2.7	88	39.5	2.0	16	2.2	0.01	96.7	1.156	83.6
T10-2cc	300	555	9	39.0	3.3	86	27.3	5.7	17	3.6	0.02	86.7		
T10-2a	300	565	11	33.3	1.6	93	26.6	2.0	7	1.4	0.02	74.0	0.969	76.3
T10-3c	450	565	9	42.0	1.4	88	17.0	0.8	14	1.4	0.04	93.3		
T10-3dc	300	565	11	36.1	3.2	87	29.0	6.0	17	1.3	0.02	80.3		
T10-5a	300	565	11	41.7	1.6	91	64.1	2.0	10	1.0	0.01	92.8		
T10-5b	300	565	11	43.9	2.0	90	66.9	4.2	11	0.9	0.01	97.7		
T10-5c	300	560	10	45.3	3.2	93	38.6	2.1	6	2.4	0.02	101	1.609	62.7
T10-6b	300	555	9	32.3	3.0	92	46.1	4.0	11	4.6	0.01	71.8	0.778	92.2
T10-6c	300	550	8	59.2	3.3	91	20.3	4.0	18	9.6	0.03	132	1.832	72.0
T10-7a	450	555	7	42.7	1.5	87	18.4	3.4	11	1.7	0.03	95.0		
T10-7b	450	560	8	38.9	2.0	90	49.7	3.6	6	1.2	0.01	86.5		
T10-7c	450	560	8	35.2	2.6	81	16.4	6.8	7	3.4	0.04	78.4		
T11-1a	300	575	13	33.8	3.1	92	40.2	0.7	19	2.0	0.02	75.2		
T11-1b	400	560	9	32.5	3.9	77	21.4	2.5	24	1.5	0.03	72.4	I	
T11-4b	450	570	10	32.8	2.2	84	29.9	2.1	17	2.1	0.02	72.9		
T11-4cc	400	565	10	29.8	2.3	80	26.4	4.8	19	2.6	0.02	66.3	I	
T14-5b1	500	570	9	30.9	1.6	89	22.6	1.4	8	0.6	0.03	68.7		
T14-5b2	450	575	11	32.5	2.0	88	22.8	1.6	12	1.3	0.03	72.4		
T14-5b3	450	570	10	34.7	1.3	88	55.1	3.9	11	0.8	0.01	77.1		
T14-5b4	520	570	8	35.1	1.8	71	12.2	19.5	15	2.2	0.05	78.1		
T16-61	400	570	11	13.3	3.7	72	25.2	4.6	16	4.8	0.02	29.5		
T16-62	400	565	10	12.9	4.1	65	16.7	5.6	18	5.5	0.03	28.7		
T16-65	500	560	7	12.5	4.7	56	8.76	5.9	22	7.9	0.05	27.8		
T17-71	450	570	10	18.4	3.2	91	48.2	1.2	23	4.1	0.01	41.0		
T21-5a	450	565	9	21.8	3.9	76	26.2	4.2	25	4.2	0.03	48.5		
T21-5b	400	570	11	22.9	2.7	81	17.8	2.7	15	5.5	0.05	50.9		
T21-5c	500	570	9	21.0	4.8	58	32.2	6.2	25	5.0	0.01	46.8		
T29-6a	300	575	13	37.4	4.3	88	33.4	2.0	13	1.1	0.02	83.2		
T29-6b	500	575	10	36.6	2.4	50	29.8	4.7	25	1.8	0.01	81.5		
T29-6cc	450	565	9	42.2	2.8	82	36.8	3.8	15	2.2	0.02	93.8	I	
T32-11	500	575	10	22.0	3.5	75	38.0	2.0	10	1.8	0.02	49.0		
T32-12	500	575	10	13.9	3.2	80	31.3	3.3	6	3.4	0.02	31.0		
T32-13	500	575	10	15.8	2.4	80	27.8	2.5	7	2.8	0.02	35.1		
T32-14	530	570	7	23.6	3.1	59	15.2	4.6	11	3.9	0.04	52.5		
T35-11	450	565	9	20.1	3.2	59	18.6	4.4	17	2.1	0.04	44.8	I	

Table 1 (*continued*)

Specimen	T_1 (°C)	T_2 (°C)	N	$B_{anc.}$ (μT)	MAD	f_{vds} (%)	q	pTRM tail	DRATs	DANG (°)	β	VADM (Z Am^2)	R	VADM$_{AARM}$ (Z Am^2)
T35-12	520	570	8	22.6	3.0	51	23.8	3.1	17	2.5	0.02	50.2		
T35-13	500	565	8	23.1	2.4	64	20.8	2.1	20	4.7	0.03	51.4		
T35-14	450	570	10	25.0	3.3	74	13.1	4.3	11	9.2	0.05	55.6	I	
T36-32	520	570	8	21.8	3.4	64	27.7	4.6	25	4.1	0.02	48.4		
T36-33	500	575	10	22.0	1.9	86	26.1	2.6	15	0.4	0.03	49.0		
T36-34	500	575	10	21.4	2.6	83	25.3	5.7	23	1.2	0.03	47.6		
TR3-c1-1	300	565	11	30.1	2.0	97	25.8	0.8	25	3.2	0.03	66.9		
TR3-c1-2	450	560	8	36.8	2.4	80	15.0	3.0	18	1.4	0.04	82.0		
TR3-c1-3	300	550	8	35.2	3.1	78	11.2	3.8	6	3.4	0.05	78.3		
TR5-e1-1	500	570	9	25.0	4.4	78	11.7	1.3	21	2.3	0.07	55.6	I	
TR5-e1-2	500	570	9	23.9	2.9	77	12.4	5.0	15	3.5	0.06	53.2	I	
TR5-e1-4	550	575	6	29.4	2.6	50	9.14	6.7	19	4.6	0.05	65.4	I	
TR6-a2-1	400	555	8	31.1	2.4	77	8.67	4.2	5	4.3	0.07	69.2		
TR6-a2-2	300	560	10	28.6	3.6	79	17.0	2.0	19	4.8	0.04	63.6		
TR6-a2-3	400	550	7	30.3	4.6	63	12.0	5.1	11	8.0	0.04	67.4		
CY-4, 781.5-1	500	570	9	59.2	3.0	70	16.8	3.5	11	2.0	0.04	132		
CY-4, 781.5-2	450	575	11	52.6	2.4	84	25.3	1.4	9	1.9	0.03	117		
CY-4, 781.5-3	500	575	10	50.6	4.0	73	23.3	6.2	15	1.8	0.03	113		
CY-4, 1034.25-1	300	570	12	23.1	3.9	83	32.2	2.5	25	4.5	0.02	51.3		
CY-4, 1034.25-2	300	575	13	24.2	3.1	87	39.5	3.8	20	4.1	0.02	53.9	1.138	47.3
CY-4, 1034.25-3	300	575	13	19.8	3.8	81	22.4	2.2	24	3.5	0.03	44.0	I	
CY-4, 1329.2-1	500	575	9	32.4	2.2	71	14.0	3.1	17	1.0	0.05	72.1		
CY-4, 1329.2-2	300	565	11	39.7	1.7	95	25.9	3.3	13	0.8	0.03	88.3		
CY-4, 1329.2-3	300	565	11	40.2	1.8	93	31.7	1.5	19	2.1	0.02	89.4		

Temperature range used in the best-fit line is between T_1 and T_2. N corresponds to the number of points used in the calculation, and $B_{anc.}$ is the resultant intensity of the field. f_{vds}, q, and β are the fraction of remanent magnetization (based on the vector difference sum), quality factor, and the degree of scattering for the chosen data points. MAD (maximum angular deviation), pTRM checks, DRATs (difference ratio sum), and DANG (deviation angle) are parameters used to assess whether chemical alteration or abnormal magnetic behavior was taking place during the experiments (Appendix A). The degree to which a given specimen was affected by remanence anisotropy is shown by R. We denoted R as I for the isotropic specimens. VADM$_{AARM}$ corresponds to the VADM corrected for anisotropic effect. None of the values are corrected for slow cooling effect. These specimens all passed the zig-zag test. Labels for the specimens from CY-4 drill site correspond to their depth (m). Note: the site labels here differ from those in [32] by the addition of the letter T, added here to distinguish the gabbro sites from the glass sites from [10].

placed in the time-series from outcrop samples. We will first address the suitability of the Troodos gabbros for paleointensity measurements.

Then we will compare the Troodos results with other published paleointensity data from a similar time interval including the results from the upper crust of Tauxe and Staudigel [10]. Finally, we will discuss the implications of the paleointensity data for the results from numerical simulations.

2. Methods

The gabbro samples were sliced into specimens 5 to 10 mm in size. These were fixed into quartz tubes and then measured in the magnetically shielded room at the paleomagnetic laboratory of the Scripps Institution of Oceanography. The Thellier–Thellier method is widely accepted for determining absolute geomagnetic intensity. In this technique, samples are repeatedly heated and cooled in zero field or in a laboratory field at progressively higher temperature steps [34]. Accurate absolute paleointensities require that the blocking and unblocking temperatures be identical (i.e., the reciprocity condition, where the magnetic carriers have single domain like behavior), and no mineralogical alteration takes place while re-heating the samples in the laboratory. To monitor the equivalence of blocking and unblocking temperatures, we performed a modified version of Thellier–Thellier method (the IZZI experiment of [35]; Fig. 2). In this method we successively heat each specimen to a given temperature. Then one of two procedures was followed. In the ZI procedure, the specimen is cooled first in zero field (Z) followed by re-heating and cooling in a 40 μT laboratory field (I). In the other procedure (IZ), the specimen is cooled first in the laboratory field, then re-heated and cooled in zero field. The laboratory field was directed along the specimen's "*Z*" axis. These IZ and ZI steps are alternated for

subsequent temperature steps. Within a given temperature step we re-heat the specimens to a lower temperature step and cool in the laboratory field to assess the change of their capacity to acquire partial thermal remanent magnetization (a pTRM check). We also performed an additional step in which we re-heated and cooled the specimens in zero field (a pTRM tail check) to assess whether the pTRM acquired at a given temperature is fully removed by cooling in zero field at the same temperature. The existence of so-called high temperature pTRM tails can perhaps better be revealed by the zig-zagging pattern in the IZZI experiment as shown in the natural remanent magnetization (NRM) versus pTRM (Arai plot, please see Appendix A for a thorough description of the analysis procedure), or in the vector end-point diagrams. We performed a total of 12 to 15 temperature steps for a total of up to 45 measurements on each specimen. The results are evaluated according to statistical criteria explained in Appendix A.

3. Results

3.1. Lower crust paleointensity results

The IZZI experiment reveals a characteristic component of magnetization unblocked in the 350–580 °C temperature range and occasionally a minor additional low-temperature (<200–300 °C) overprint magnetization (see insets to Fig. 2). The typical maximum unblocking temperatures are near 580 °C. The magnetic carriers demonstrate a relatively high coercivity spectra (median destructive field of 45 mT) [32]. These characteristics suggest that the magnetic carrier of the Troodos gabbros is an oxyexsolved low-Ti titanomagnetite of single to perhaps small pseudo-single domain grain size.

From the entire specimen collection, ninety one samples passed all criteria (examples are shown in Fig. 2). The results were then averaged by site. Our sampled sites are located hundreds to thousands of meters apart, implying that each site mean is likely to represent a distinct cooling unit.

The sources for paleointensity variations within a given site include alteration, measurement errors, or remanence anisotropy. Both alteration and measurement errors can be detected by the various statistical criteria (Appendix A). The relative orientation of the remanence anisotropy tensor and the direction of the laboratory field controls the way in which the anisotropy effects the resultant paleointensity value (Appendix A, [36]). Our drilled cores and sliced specimens were randomly oriented with respect to one another, which results in a random anisotropic effect. Therefore, sites showing a well grouped paleointensity results (i.e., the results deviate less than 25% or 5 μT from the site mean) are unlikely to be biased by anisotropy. For specimens with a higher degree of variation relative to their site mean, we determined the remanence anisotropy and corrected the paleointensity estimate following [36]. The correlation between the degree of deviation from the site mean and the degree to which a given specimen is effected by anisotropy (R, Table 1) further confirms the assumption that significant remanence anisotropy is manifested by substantial within-site paleofield scatter. Sites with within-site variability greater than 25% or 5 μT even after the remanence anisotropy correction were eliminated from further consideration.

We consider only sites that have at least three specimens. After examination of the consistency of the results within and among specimens from a given site, we are left with 18 high-quality sites, with a total of 80 specimens (Fig. 3, Tables 1 and 2). The average virtual axial dipole moment (VADM), unadjusted for slow cooling, for the gabbros is 67 ± 24 Z Am^2 (paleolatitude of 20° [37]). The variations in the dipole moments are up to 35% of the mean and are similar to the Cenozoic magnetic field variations [16].

Within our acceptable data set, eight gabbroic sites are located within a single tectonically undisrupted domain (Fig. 1) and can be used to examine temporal variations of the geomagnetic field (Fig. 3a). The paleointensity data from these sites exhibit considerable serial correlation and appear to define a quasi-cyclic geomagnetic field variation along the 11 km of the lower oceanic crust. Assuming a full spreading rate of 20 to 75 mm/yr [23–27], this corresponds to 0.3 to 1.1 Ma of accretion.

3.2. Upper crust paleointensity analysis

In addition to the time-series from the gabbro samples presented in the foregoing, Tauxe and Staudigel [10] presented data from submarine basaltic glasses (SBG) obtained from two transects through the Troodos extrusive section providing two independent temporal views of the CNS magnetic field (Fig. 1). These transects are located east of our gabbro sequence and consequently record different, most likely earlier times of the CNS field. The two transects are 10 km apart along the spreading direction, implying an age difference of some 0.2 to 1 Ma (Fig. 1). Each transect contains up to ten geochemically distinctive units [38] creating a time-series that might span as much as 10^5 yrs [39]. The actual time interval between the various pillow lava flows is

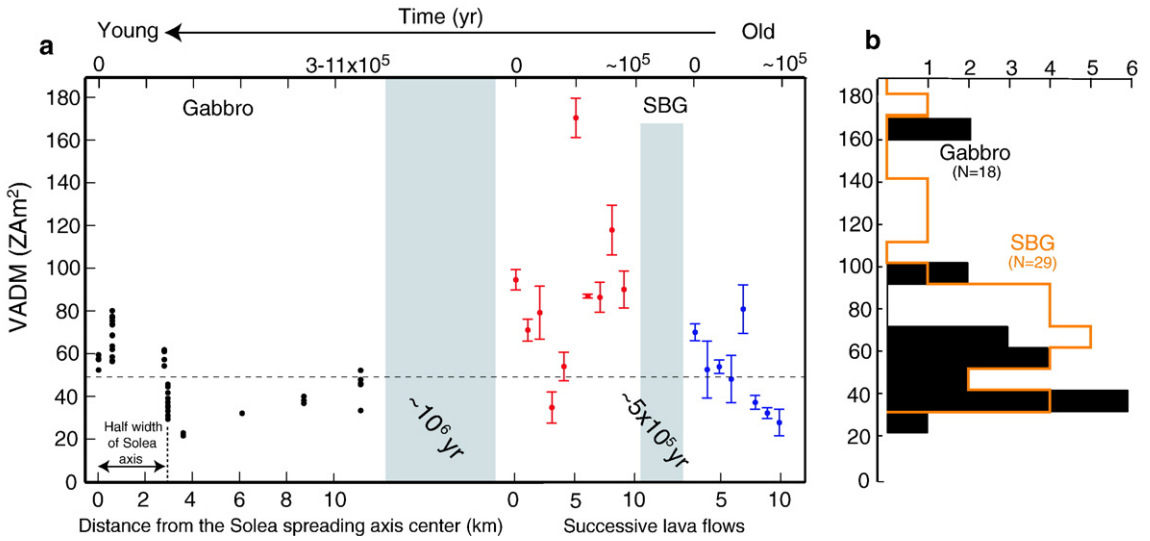

Fig. 3. Summary of paleointensity data from the Troodos ophiolite. All results were converted to VADM (assuming a paleolatitude of 20° [37]). (a) Three time-series of the magnetic dipole moments during the late CNS from the gabbros and glasses [10]. Gray areas represent gaps in time estimated from moderate spreading rate (full spreading rate of 20 to 75 mm/yr). Results for the gabbro specimens are shown as individual points and are corrected for cooling rate and anisotropy (see text for details). Results for the SBG sites correspond to the average results from successive cooling units (color scheme same as in Fig. 1b). Dashed line represents the average field of the Cenozoic [16]. (b) Histograms of all paleointensity data available from the upper [10] and lower Troodos crust. Data counts are from individual sites. Results for the gabbros are corrected for cooling rate.

unknown. From the original work of [10], we have used only those data points whose age relations were known from stratigraphic order and conformed to our selection criteria (Fig. 3a). Glasses from dikes have been excluded from consideration. These two time-series, although more scattered than the gabbroic series, also appear to exhibit serial correlation. Their grand mean averaged VADM was reported as 75± 41 Z Am^2 whereas the mean VADM of the data subset used here is 77±36 Z Am^2.

Table 2
Summary of site statistics based on the results shown in Table 1

Site	Lat. (°N)	Long. (°E)	N	$\bar{B}$ (μT)	σ_B	$100(\sigma/\bar{B})$	VADM (Z Am^2)	σ_{VADM}
T5	34.5376	32.5023	10	21.3	3.0	7.8	37.8	5.4
T6	34.5545	32.4905	6	55.5	6.8	12.2	98.8	12.1
T8	34.5416	32.5916	5	26.9	5.2	19.5	47.8	9.3
T10	34.5307	32.5247	13	38.0	4.6	12.1	65.7	10.3
T11	34.5342	32.5210	4	32.2	1.7	5.3	57.3	3.0
T14	34.5359	32.5395	4	33.3	2.0	5.9	59.2	3.4
T16	34.5279	32.5438	3	12.9	0.4	3.1	22.9	0.7
T21	34.5362	32.5763	3	21.9	1.0	4.3	38.9	1.6
T29	34.5249	33.0302	3	38.7	3.0	7.8	68.9	5.3
T32	34.5222	33.0479	4	18.8	4.7	24.9	33.5	8.3
T35	34.5423	33.0104	4	22.7	2.0	8.8	40.4	3.5
T36	34.5361	33.0168	3	21.7	0.3	1.4	38.6	0.5
TR3	34.5826	32.5576	3	34.0	3.5	10.2	60.6	6.2
TR5	34.5547	32.4741	3	26.1	2.9	11.1	46.4	5.1
TR6	34.5612	32.4726	3	30.0	1.3	4.2	53.3	2.2
CY-4, 781.5	33.0538	34.5406	3	54.1	4.5	8.3	96.5	8.0
CY-4, 1034.25	33.0538	34.5406	3	21.4	1.7	7.7	39.7	4.1
CY-4, 1329.2	33.0538	34.5406	3	37.4	4.4	11.6	66.6	7.7

N are the number of specimens used in the calculation. The averaged field values ($\bar{B}$, σ_B) are not corrected for cooling rate, whereas the virtual axial dipole moment (VADM, λ=20°) are corrected for cooling rate ($\mathrm{VADM}_{\mathrm{corrected}}$=0.8 VADM).

4. Discussion

Rapidly cooled igneous rocks (e.g., SBG) record the variability of the geomagnetic field with virtually no averaging involved, whereas slowly cooled rocks (e.g., gabbros) should filter out the short wavelength changes of the field. Furthermore, the ratio between the cooling rates of plutonic rocks during formation and in the laboratory results in an overestimation of the ancient geomagnetic field [40]. SBG cools in nature at a similar cooling rate as in the laboratory [41], and consequently require no significant cooling rate correction. Direct measurements from the lower crust at the Mid-Atlantic Ridge [42] and thermal modeling [43] suggest that lower oceanic crustal cooling (over the 600 to 300 °C temperature range relevant for our paleointensity estimates) may require up to 10^5 yrs. These cooling rates are significantly slower than in the laboratory and would equate to overestimates of the ancient field by 40% [44,36]. Actual cooling rates for the Troodos gabbros are poorly constrained but might be significantly faster, for example due to hydrothermal circulation. We have arbitrarily corrected the gabbro paleointensity estimates by a factor of 0.8, corresponding to a 20% overestimate of the ancient field. Since we are primarily concerned with paleointensity variations, the precise cooling rate correction is not critical although cooling rate variations might account for up to 10% of the between-site paleointensity variations. Since the cores within each sites are located a few meters apart, and there were no petrographic (i.e., grain size) or any field indications for a thermal boundary, we conclude that cooling rate variations within a single site are unlikely and therefore cannot explain within-site paleointensity variations.

The cooling rate corrected gabbro results range from 23 to 96 Z Am^2 (Fig. 4 and Table 2), and the corrected average VADM of the gabbros is 54±20 Z Am^2. This value, although statistically indistinguishable, is lower than the extrusive averaged dipole moment. We speculate that the reason for the difference is that the portions of the crust discussed here sample different time intervals, and therefore record different time-series of the geomagnetic field.

By considering all three time-series, it is possible to place constraints on the variability of the geomagnetic field during the CNS in a more definitive manner than heretofore possible. Discrepancies noted in the published data, especially in those studies that had few data points, are plausibly attributed to under-sampling of the true geomagnetic field variability, with some studies sampling peaks of the geomagnetic field [e.g., [9]] and others sampling low points [e.g., [7]].

The observed trend in the gabbros is also interesting when taking into account the slow to intermediate spreading environment in which the Troodos crust formed. The quasi-continuous VADM trend is suggestive of a relatively continuous lower crust formation with negligible re-heating events, if any, after the initial cooling within the accretion zone.

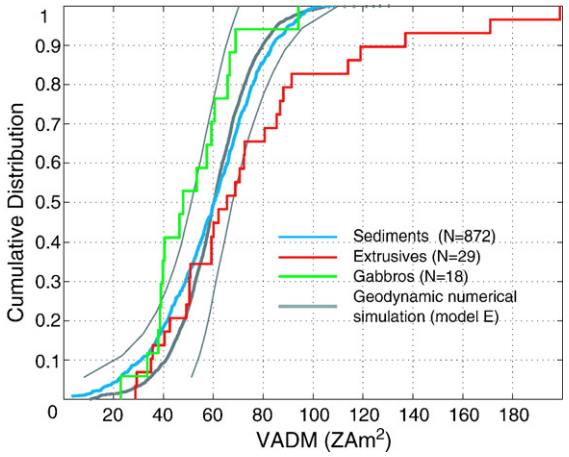

Fig. 4. Distributions of dipole moments from the late CNS. Heavy gray line corresponds to the geodynamo numerical simulation results [model E [2]]. The 95% confidence bounds (fine gray lines) for the numerical simulation were determined from CDFs for a large number of pseudo-samples (each with 18 samples as for the Troodos gabbros data) drawn from the simulation. Gabbros (corrected for cooling rate) and glasses [10] results are shown in green and red, respectively. The median of the sediment record (blue, [15]) is adjusted to the median of the numerical simulation data. In brackets are the number of cooling units that are used in the calculation. (For interpretation of the references to colour in this figure legend, the reader is referred to the web version of this article.)

4.1. Comparison with other data sets and geodynamo numerical simulations

Cumulative distributions of VADM data allow us to compare the Troodos data sets and the geodynamo model predictions (Fig. 4). We use for comparison Model E of Glatzmair et al. [2] as it is the only model which shows no reversals throughout the 300 kyr simulation and best represents the CNS. The mean values for extrusives (75 Z Am^2), intrusives (54 Z Am^2), and the geodynamo numerical simulations (60 Z Am^2) are quite similar, and are comparable to the post-CNS average intensity field [16,13]. The apparent concordance of our results with the model is artificial, however, because Glatzmaier et al. [2] argue that the true average of their numerical simulations must be higher owing the computational necessity of using unrealistically high outer core viscosities. The paleointensity data from Troodos include a substantial number of sites, both from extrusive and intrusive rocks. The spatial distribution of these sites, together with the time averaging inherent in

slowly cooled gabbros, should provide a robust estimate of the geomagnetic field in the latter part of the CNS. To the extent that these data are representative, we conclude that an average value for the late CNS dipole moment much higher than ~60–70 Z Am^2 is unlikely.

The comparison between the data sets also allows us to consider the variability of intensity values in the late CNS. For this purpose, we plot the sedimentary relative paleointensity data of Cronin et al. [15], adjusted to a common median value with the numerical simulation data. The sedimentary and intrusive data sets have remarkably similar distributions, and display much less variability than the extrusives. We attribute this to the fact that both intrusive and sedimentary samples average the geomagnetic field over some period of time while extrusives are more likely to represent "snap shots" of field intensities. Also, specimens of SBG are weakly magnetized and instrumental noise means that the weakest specimens are never measured, resulting in a possible bias in SBG data toward higher field values. Therefore, the variability of the geomagnetic field during the late CNS was significantly higher than that predicted by the numerical simulations.

5. Conclusions

The paleointensity results from 18 sites in the lower Troodos crust shown here, together with previously published results from the upper Troodos crust provide three independent time-series of absolute paleointensities from the CNS. The serial correlation of the data provides an independent confirmation of the quality of our results and agrees with the available sediment and extrusive records. The observed quasi-continuous paleointensity trend in the lower Troodos crust also suggests relatively continuous cooling of the lower crust.

The high variability of the paleointensity data from the Troodos ophiolite may offer an explanation for the wide range of paleofield estimates previously reported from the CNS. Based on the mean value of 54± 20 Z Am^2 we suggest that the geomagnetic field was weaker and more variable than the predictions made by the geodynamo numerical simulations. This result can be used to refine the geodynamo numerical simulations.

Acknowledgments

We thank G. Glatzmair for providing the geodynamic numerical modeling results for comparison with our data. We also thank A. Agnon, M. Abelson, and R. J. Varga for kindly allowing us to use their specimens. The manuscript was greatly improved by the constructive comments of the editor M.L. Delaney and by the comments of two anonymous reviewers. This work was partially supported by the National Science Foundation grant OPP-0229403.

Appendix A. Analysis of IZZI results

The results from the IZZI experiment are assessed according to the following reliability criteria (see Lecture 10 of http://earthref.org/MAGIC/books/Tauxe/2005/ for more details). At least five data points are needed in the calculation. The best-fit lines to the progressive thermal demagnetization vectors are calculated using principal component analysis [45]. The maximum angular deviation (MAD) about the characteristic magnetization vector (ChRM) of the chosen points has to be less than 15°. The

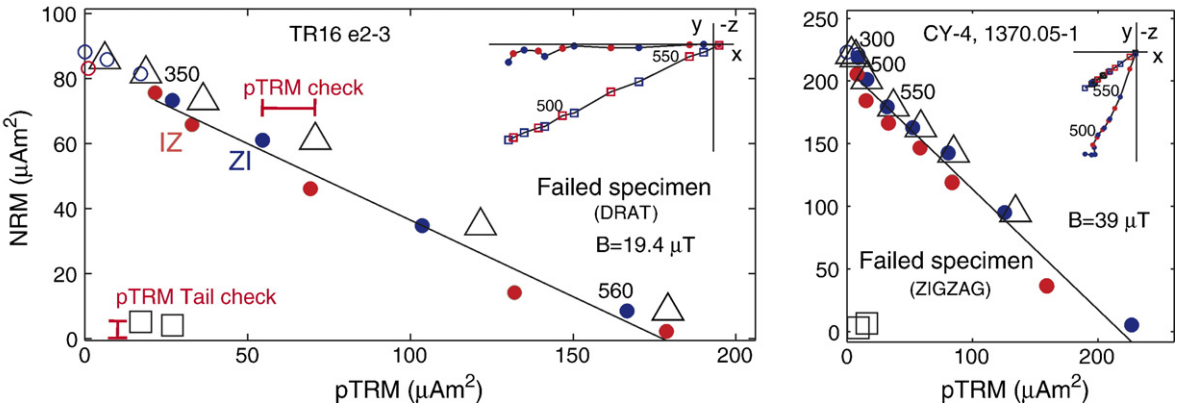

Fig. 5. Representative illustrations of the selection criteria that were used to evaluate the quality of the measurements. Blue (red) symbols represent the ZI (IZ) steps. The slopes and the vectorial directions of both ZI and IZ populations are compared to assess whether the specimens are uniformly magnetized. Open triangles and squares indicate the pTRM checks and pTRM-tail checks, respectively. Both specimens demonstrate unacceptable results due to high DRAT (left) and failure of the zig-zag test (right). (For interpretation of the references to colour in this figure legend, the reader is referred to the web version of this article.)

ChRM has to point toward the origin with a deviation angle (DANG) of less than 10°. In the NRM–pTRM plots (i.e., Arai plots), the best-fit line through the chosen data points must have low scatter around the mean [46], ($\beta = \sigma / |b| < 0.1$). We sum all the differences between the pTRM checks and the corresponding original pTRM and normalized it by the pTRM gained in the temperature range used for the paleofield determination. This difference ratio sum (DRATs) must be less than or equal to 25% in order to avoid the use of specimens that developed chemical alteration during the experiment. The fraction of remanent magnetization (f_{vds}, vector difference sum) was always greater than 50%.

We use a new parameter to quantify the degree of "zig-zagging" observed in the IZZI experiment. Here we assess the zig-zagging nature of the specimens by evaluating the slopes of the ZI and IZ data points separately. The results of a given specimen are thought to be of a good quality if these slopes are statistically distinct at the 95% confidence level (using the test for common mean of [47]) (Fig. 5). This evaluation of the zig-zagging nature does not require a threshold limit, but produces an independent fail/pass criteria.

We have used pTRM tail checks [48] in the lower temperature range (<300 °C) where it had to be less than 5% and the zig-zagging parameter above this temperature range. In cases where it was needed, the paleointensities were corrected for the anisotropy of remanence as follows [36]:

$$B_{\text{corrected}} = R/B_{\text{anc}} \tag{1}$$

where R is:

$$R = \frac{|\chi \cdot \hat{H}_{\text{anc}}|}{|\chi \cdot \hat{H}_{\text{lab}}|} \tag{2}$$

and χ is the remanence anisotropy tensor, $\hat{H}_{\text{anc}}$ is the ancient field direction determined from the ChRM direction and the anisotropy tensor, and $\hat{H}_{\text{lab}}$ is the lab field direction applied along the sample Z coordinate axis.

References

[1] R.T. Merrill, M.W. McElhinny, P.L. McFadden, The Magnetic Field of the Earth: Paleomagnetism, the Core, and the Deep Mantle, Int. Geophys. Ser., Academic, San Diego, Calif., 1996.

[2] G.A. Glatzmaier, R.S. Coe, L. Hongre, P.H. Roberts, The role of the Earth's mantle in controlling the frequency of geomagnetic reversals, Nature 401 (1999) 885–890.

[3] J. Bloxham, Sensitivity of the geomagnetic axial dipole to thermal core–mantle interactions, Nature 405 (2000) 63–65.

[4] J.E.T. Channell, M. Erba, E. Nakanashi, K. Tamaki, Late Jurassic–early Cretaceous time scales and oceanic magnetic anomaly block models, in: W. Berggren, D.V. Kent, M. Aubry, J. Hardenbol (Eds.), Geochronology, Time Scales and Global Stratigraphic Correlation, Soc. Sed. Geol., vol. 54, 1995, pp. 51–63.

[5] S.C. Cande, D.V. Kent, Revised calibration of the geomagnetic polarity timescale for the late Cretaceous and Cenozoic, J. Geophys. Res. 100 (1995) 6093–6095.

[6] P. Riisager, J. Riisager, X.X. Zhao, R.S. Coe, Cretaceous geomagnetic paleointensities: Thellier experiments on pillow lavas and submarine basaltic glass from the Ontong Java Plateau, Geochem. Geophys. Geosyst. 4 (12) (2003), doi:10.1029/2003GC000611.

[7] H.F. Tanaka, M. Kono, Paleointensities from a Cretaceous basalt platform in inner Mongolia, northeastern China, Phys. Earth Planet. Inter. 133 (2002) 147–157.

[8] J.A. Tarduno, R.D. Cottrell, A.V. Smirnov, The Cretaceous superchron geodynamo: observations near the tangent cylinder, Proc. Natl. Acad. Sci. U. S. A. 99 (2002) 14020–14025.

[9] J.A. Tarduno, R.D. Cottrell, A.V. Smirnov, High geomagnetic intensity during the mid-Cretaceous from Thellier analyses of single plagioclase crystals, Science 291 (2001) 1779–1783.

[10] L. Tauxe, H. Staudigel, Strength of the geomagnetic field in the Cretaceous normal superchron: new data from submarine basaltic glass of the Troodos ophiolite, Geochem. Geophys. Geosyst. 5 (2) (2004), doi:10.1029/2003GC000635.

[11] X.X. Zhao, P. Riisager, J. Riisager, U. Draeger, R.S. Coe, Z. Zheng, New palaeointensity results from Cretaceous basalt of inner Mongolia, China, Phys. Earth Planet. Inter. 141 (2004) 131–140.

[12] T. Pick, L. Tauxe, Geomagnetic palaeointensities during the Cretaceous normal superchron measured using submarine basaltic glass, Nature 366 (1993) 238–242.

[13] L. Tauxe, Long-term trends in paleointensity: the contribution of DSDP/ODP submarine basaltic glass collections, Phys. Earth Planet. Inter. 156 (2006) 223–241.

[14] A. Kurazhkovskii, N. Kurazhkovskaya, B. Klain, A. Guzhikov, Paleointensity behavior in Barremian–Cenomanian (Cretaceous), Int. J. Geomagn. Aeron. 5 (2004), doi:10.1029/2003GI000043.

[15] M. Cronin, L. Tauxe, C. Constable, P.A. Selkin, T. Pick, Noise in the quiet zone, Earth Planet. Sci. Lett. 190 (2001) 13–30.

[16] P.A. Selkin, L. Tauxe, Long-term variations in paleointensity, Philos. Trans. R. Soc. Lond., A 358 (2000) 1065–1088.

[17] J.A. Tarduno, R.D. Cottrell, Dipole strength and variation of the time-averaged reversing and nonreversing geodynamo based on Thellier analyses of single plagioclase crystals, J. Geophys. Res. 110 (2005), doi:10.1029/2005JB003970.

[18] J.P. Valet, Time variations in geomagnetic intensity, Rev. Geophys. 41 (1) (2003), doi:10.1029/2001RG000104.

[19] S.C. Cande, D.V. Kent, Ultrahigh resolution marine magnetic anomaly profiles: a record of continuous paleointensity variations? J. Geophys. Res. 97 (1992) 15075–15083.

[20] J.S. Gee, S.C. Cande, J.A. Hildebrand, K. Donnelly, R.L. Parker, Geomagnetic intensity variations over the past 780 kyr obtained from near-seafloor magnetic anomalies, Nature 408 (2000) 827–832.

[21] J. Bowles, L. Tauxe, J. Gee, D. McMillan, S.C. Cande, Source of tiny wiggles in chron C5: a comparison of sedimentary relative intensity and marine magnetic anomalies, Geochem. Geophys. Geosyst. 4 (6) (2003), doi:10.1029/2002GC000489.

[22] S.B. Mukasa, J.N. Ludden, Uranium–lead isotopic ages of plagiogranites from the Troodos ophiolite, Cyprus, and their tectonic significance, Geology 15 (1987) 825–828.

[23] E.M. Moores, F.J. Vine, Troodos massif, Cyprus and other ophiolites as oceanic crust — evaluation and implications, Philos. Trans. R. Soc. Lond. Ser. 268A (1971) 443–466.

[24] S.D. Hurst, E.M. Moores, R.J. Varga, Structural and geophysical expression of the Solea graben, Troodos ophiolite, Cyprus, Tectonics 13 (1) (1994) 139–156.
[25] C. Small, Global systematics of mid-ocean ridge morphology, in: R. Buck, P. Delaney, J.A. Karson, Y. Lagabrielle (Eds.), Faulting and Magmatism at Mid-Ocean Ridges, Geophys. Mon. Ser., vol. 106, Am. Geophys. Union, Washington, D.C., 1998, pp. 1–26.
[26] R.J. Varga, J.S. Gee, L. Bettison-Varga, R.S. Anderson, C.L. Johnson, Early establishment of seafloor hydrothermal systems during structural extension: paleomagnetic evidence from the Troodos ophiolite, Cyprus, Earth Planet. Sci. Lett. 171 (2) (1999) 221–235.
[27] P.A. Rona, Hydrothermal mineralization at seafloor spreading centers, Earth-Sci. Rev. 20 (1984) 1–104.
[28] J.M. Sinton, R.S. Detrick, Mid-ocean ridge magma chambers, J. Geophys. 97 (B1) (1992) 197–216.
[29] R.J. Varga, E.M. Moores, Spreading structure of the Troodos ophiolite, Cyprus, Geology 13 (1985) 846–850.
[30] C.J. Macleod, A.H.F. Robertson, S. Allerton, P. Browning, I.G. Gass, R.N. Taylor, F.J. Vine, C. Xenophontos, Tectonic evolution of the Troodos ophiolite within the Tethyan framework — comment, Tectonics 11 (1992) 910–915.
[31] C.J. Macleod, S. Allerton, I.G. Gass, C. Xenophontos, Structure of a fossil ridge-transform intersection in the Troodos ophiolite, Nature 348 (1990) 717–720.
[32] R. Granot, M. Abelson, H. Ron, A. Agnon, The oceanic crust in 3D: paleomagnetic reconstruction in the Troodos ophiolite gabbro, Earth Planet. Sci. Lett. 251 (2006) 280–292.
[33] N. Bonhommet, P. Roperch, F. Calza, Paleomagnetic arguments for block rotations along the Arakapas fault (Cyprus), Geology 16 (1988) 422–425.
[34] R.S. Coe, Paleointensities of earths magnetic field determined from Tertiary and Quaternary rocks, J. Geophys. Res. 72 (1967) 3247–3262.
[35] Y.J. Yu, L. Tauxe, A. Genevey, Toward an optimal geomagnetic field intensity determination technique, Geochem. Geophys. Geosyst. 5 (2) (2004), doi:10.1029/2003GC000630.
[36] P.A. Selkin, J.S. Gee, L. Tauxe, W.P. Meurer, A.J. Newell, The effect of remanence anisotropy on paleointensity estimates: a case study from the Archean Stillwater complex, Earth Planet. Sci. Lett. 183 (2000) 403–416.
[37] T.M.M. Clube, K.M. Creer, A.H.F. Robertson, Paleorotation of the Troodos microplate, Cyprus, Nature 317 (1985) 522–525.
[38] M. Rautenschlein, G.A. Jenner, J. Hertogen, A.W. Hofmann, R. Kerrich, H.U. Schmincke, W.M. White, Isotopic and trace element composition of volcanic glasses from the Akaki canyon, Cyprus: implications for the origin of the Troodos ophiolite, Earth Planet. Sci. Lett. 75 (1985) 369–383.
[39] H.U. Schmincke, M. Rautenschlein, P.T. Robinson, J.M. Mehegan, Troodos extrusive series of Cyprus: a comparison with oceanic crust, Geology 11 (1983) 405–409.
[40] S.L. Halgedahl, R. Day, M. Fuller, The effect of cooling rate on the intensity of weak-field TRM in single-domain magnetite, J. Geophys. Res. 85 (7) (1980) 3690–3698.
[41] J. Bowles, J.S. Gee, D.V. Kent, E. Bergmanis, J. Sinton, Cooling rate effects on paleointensity estimates in submarine basaltic glass and implications for dating young flows, Geochem. Geophys. Geosyst. 6 (7) (2005), doi:10.1029/2004GC000900.
[42] J. Gee, W.P. Meurer, Slow cooling of middle and lower oceanic crust inferred from multicomponent magnetizations of gabbroic rocks from the Mid-Atlantic ridge south of the Kane fracture zone (MARK) area, J. Geophys. Res. 107 (7) (2002), doi:10.1029/2000JB000062.
[43] W.J. Shaw, J. Lin, Models of ocean ridge lithospheric deformation: dependence on crustal thickness, spreading rate, and segmentation, J. Geophys. Res. 101 (B8) (1996) 17977–17993.
[44] G. Pullaiah, E. Irving, K.L. Buchan, D.J. Dunlop, Magnetization changes caused by burial and uplift, Earth Planet. Sci. Lett. 28 (1975) 133–143.
[45] J.L. Kirschvink, The least-squares line and plane and the analysis of paleomagnetic data, Geophys. J. R. Astron. Soc. 62 (1980) 699–718.
[46] R.S. Coe, S. Gromme, E.A. Mankinen, Geomagnetic paleointensities from radiocarbon-dated lava flows on Hawaii and question of Pacific nondipole low, J. Geophys. Res. 83 (1978) 1740–1756.
[47] G.S. Watson, Large sample theory of the Langevin distributions, J. Stat. Plan. Inference 8 (1983) 245–256.
[48] P. Riisager, J. Riisager, Detecting multidomain magnetic grains in Thellier palaeointensity experiments, Phys. Earth Planet. Inter. 125 (2001) 111–117.